Journal of Chemical&Engineering Data

pubs.acs.org/jced

Article

Phase Equilibria of Carbon Dioxide and Methane Gas Hydrates in the Presence of Tetramethylammonium Chloride and Tetrapropylammonium Bromide-Based Deep Eutectic Solvents

Njabulo Mziwandile Zulu,* Hamed Hashemi, and Kaniki Tumba

Cite This: J. Chem. Eng. Data 2025, 70, 3665−3674

Read Online

ABSTRACT: The effects of four deep eutectic solvents (DESs) on the phase equilibrium conditions of CO_2 and CH_4 gas hydrates were investigated. The mixtures of tetramethylammonium chloride (TMAC) and tetrapropylammonium bromide (TPAB) as hydrogen-bond acceptors with glycerol and ethylene glycol (EG) as hydrogen-bond donors were used to formulate the DESs. The combinations of TMAC/glycerol, TMAC/EG, TPAB/glycerol, and TPAB/EG were all made at a 1:3 molar ratio. The concentrations of DESs in the aqueous solutions were 2 and 4 wt %. The hydrate dissociation conditions for CO_2 and CH_4 systems were measured using an isochoric pressure-search method in the temperature ranges of (277.85 to 282.97) K and (276.03 to 285.15) K, respectively, and pressure ranges of (2.03 to 5.28) MPa and (3.71 to 10.39) MPa, respectively. All the studied DESs demonstrated the thermodynamic gas hydrate inhibition effect on CO_2 and CH_4 hydrate formation. The gas hydrate inhibition ability ranking from the highest to the lowest was found to be in the order of: TMAC/glycerol > TMAC/EG > TPAB/glycerol > TPAB/EG. This result proved that DESs have great potential to be effective green thermodynamic hydrate inhibitors.

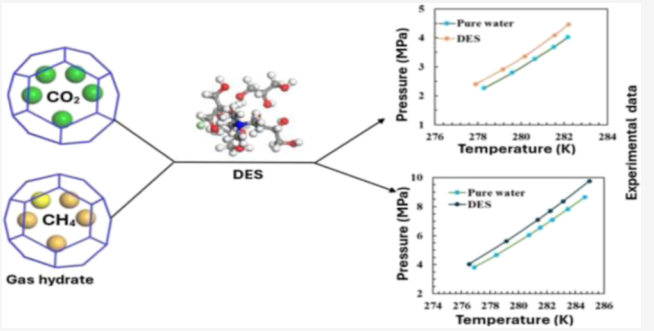

INTRODUCTION

Gas hydrates consist of guest molecules of gas which are entrapped inside the host molecules of water and their formation takes place under low-temperature and high-pressure conditions.[1] Some of the gases which commonly form hydrates are methane, carbon dioxide, propane, ethane, and hydrogen sulfide.[1] Formation of gas hydrates is one of the major problems in the production, processing, and transportation of natural gases because of their crystalline and nonflowing nature. Their presence may plug the gas transmission lines which may pose a safety risk and lead to financial loss.[2] Therefore, it is in the interest of oil and gas industry to urgently search for cost-effective and environmentally friendly measures to prevent their formation.

Different techniques are employed in mitigating the formation of gas hydrates and these include thermal heating, depressurization, dehydration, and chemical methods.[3] Among these methods, chemical inhibition is the most economical and cost-effective approach as it prevents the formation of gas hydrate without disturbing the normal flow inside the pipeline.[4] Chemical inhibition is classified into two major types which are thermodynamic hydrate inhibitors (THIs) and kinetic hydrate inhibitors (KHIs).[5] The addition of thermodynamic hydrate inhibitors shifts the hydrate formation conditions to higher pressure and lower temperature regions, while the kinetic hydrate inhibitors delay the formation of gas hydrates.[6] The selection criterion of the inhibition approach is based on the economical, safety, and environmental considerations.[1,7,8] The conventional method for the inhibition of gas hydrates is the thermodynamic approach; however, its application is limited by some few drawbacks associated with its use which include high cost and negative environmental impact.[1] The poor performance of KHIs at high pressure, high subcooling, and high-water cut conditions has led researchers to continuously search for cost-effective and environmentally friendly THIs.[5,9]

Ionic liquids have recently attracted interest in this research area because of their strong electrostatic charges and tunable properties which could be altered to form hydrogen bonding with water.[10] However, their industrial application has been limited by their own disadvantages which include high cost, toxicity, combustible nature, poor biodegradability, and high viscosity related to their utilization.[11−15] Consequently, deep

Received: December 30, 2024
Revised: July 15, 2025
Accepted: August 6, 2025
Published: August 14, 2025

https://doi.org/10.1021/acs.jced.4c00744
J. Chem. Eng. Data 2025, 70, 3665−3674

eutectic solvents (DESs) which are known for their cost-effectiveness, nontoxicity, and biodegradable nature have been discovered as the next generation of green solvents. These solvents could be a sound alternative to the currently used costly and environmentally unfriendly gas hydrate inhibitors because they have similar physicochemical properties to ionic liquids.[16]

Generally, DESs are binary or ternary mixtures obtained from components of quaternary ammonium salts as hydrogen-bond acceptors (HBAs) and hydrogen-bond donors (HBDs).[17] The eutectic mixture formed usually has lower melting point and higher density than the individual components. DESs have been proposed by several researchers to be potential green solvents for the removal of harmful impurities and the prevention of flow assurance issues such as the gas hydrate formation in oil and gas industry.[18] The gas hydrate inhibition effect of DESs was first reported by Lee et al.[19] They investigated the effect of choline chloride and urea-based DESs on methane gas hydrates. The potential of the investigated DESs as thermodynamic hydrate inhibitors was demonstrated. In a similar study, Sivabalan et al.[20] identified tetraethylammonium acetate and tetraethylammonium bromide-based DESs as thermodynamic inhibitors for carbon dioxide hydrate formation. Further work by Khoo et al.[21] displayed a dual inhibition effect of reline DES on nucleation and formation of methane hydrates and thus acting as both kinetic and thermodynamic inhibitors. Moreover, Rasool et al.[22] studied the effect of choline chloride and urea-based DES on methane gas hydrates and found that the addition of DES inhibited the hydrate formation.

It is evident from these few studies that the phase equilibrium data related to the gas hydrate-forming systems in the presence of DESs is limited. This is likely to hinder the investigation of the inhibition effect of DESs on gas hydrate formation. Hence, more work is still required to validate DESs as gas hydrate inhibitors. This study is aimed at investigating the effectiveness of selected variety of deep eutectic solvents in preventing the formation of carbon dioxide and methane gas hydrates. Once their effectiveness is established, they could be introduced into industrial application to address the current gap of cost-effective and environmentally friendly inhibitors.

In this work, the effects of tetramethylammonium chloride (TMAC) and tetrapropylammonium bromide (TPAB)-based DESs on equilibrium conditions of carbon dioxide and methane clathrate hydrates are investigated. There are four DESs that are synthesized and characterized from a combination of ethylene glycol and glycerol as the HBDs and TMAC and TPAB as the HBAs. The combinations of TPAB/glycerol, TPAB/ethylene glycol, TMAC/glycerol, and TMAC/ethylene glycol were formed at a 1:3 molar ratio, respectively. The experimental hydrate dissociation conditions for the carbon dioxide + DES + water and methane + DES + water systems are reported in the temperature ranges of (277.85 to 282.97) K and (276.03 to 285.15) K, respectively, and pressure ranges of (2.03 to 5.28) MPa and (3.71 to 10.39) MPa, respectively. The concentrations of DES in the aqueous solutions are 0.02 and 0.04 mass fractions. The hydrate dissociation data was measured, and average suppression temperatures were calculated to understand the extent of thermodynamic gas hydrate inhibition illustrated by the studied DESs. The dissociation enthalpies (ΔH_{diss}) for carbon dioxide and methane gas hydrates were also estimated in this study.

EXPERIMENTAL METHODS

Materials. Materials used for this study are outlined in Table 1 and they include distilled water, carbon dioxide, methane, and DESs. Distilled water was obtained from the research laboratory at Mangosuthu University of Technology (MUT) where this work was conducted. All the gases were supplied by AFROX (South Africa). All the DES components were supplied by SIGMA-Aldrich. The chemical structures of DES constituents are shown in Table 2.

Table 1. Supplier, Purity, and CAS Registry Number of Chemicals Used[a]

chemical	supplier	purity (mass fraction)[a]	CAS no.
tetrapropylammonium bromide	Sigma-Aldrich	≥0.980	1941-30-6
tetramethylammonium chloride	Sigma-Aldrich	≥0.980	75-57-0
ethylene glycol	Sigma-Aldrich	≥0.990	107-21-1
glycerol	Sigma-Aldrich	≥0.995	56-81-5
methane	Afrox-SA	0.995[b]	
carbon dioxide	Afrox-SA	0.999[b]	124-38-9
water	MUT	≥0.999	7732-18-5

[a]No additional purification was done; water content for TPAB, TMAC, EG, and glycerol was 3.8×10^{-4}, 3.9×10^{-4}, 4.2×10^{-4}, and 4.5×10^{-4}, respectively. [b]Mole fraction.

Table 2. Chemical Structures of the DES Constituents Used in This Work

Chemical Name	Chemical Formula	Chemical Structure
Hydrogen Bond Acceptors		
Tetramethylammonium Chloride	$C_4H_{12}N.Cl$	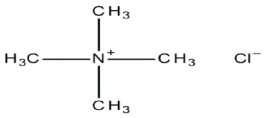
Tetrapropylammonium Bromide	$C_{12}H_{28}N.Br$	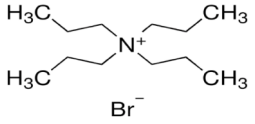
Hydrogen Bond Donors		
Glycerol	$C_3H_8O_3$	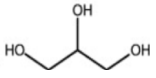
Ethylene Glycol	$C_2H_6O_2$	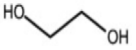

Experimental Apparatus and Procedure. *Preparation and Characterization of DESs.* The DESs were prepared and characterized at the MUT research lab, and their typical compositions are listed in Table 3. An accurate analytical balance, model AS220/C/2 (supplied by RADWAG, Poland) with an uncertainty of $\pm 1 \times 10^{-7}$ kg in mass, was used to prepare DESs having an uncertainty level of $\pm 5 \times 10^{-7}$ m^3 gravimetrically.

The preparation and purification of DESs were carried out using the procedure described by several researchers in the

https://doi.org/10.1021/acs.jced.4c00744
J. Chem. Eng. Data 2025, 70, 3665−3674

Table 3. Compositions and Abbreviations for the Studied DESs

molar ratio	abbreviation
1 TPAB:3 glycerol	DES 1
1 TPAB:3 ethylene glycol	DES 2
1 TMAC:3 glycerol	DES 3
1 TMAC:3 ethylene glycol	DES 4

literature.[23−25] The investigated DESs were prepared by mixing the hydrogen-bond acceptor (HBA) with hydrogen-bond donor (HBD) according to the desired HBA-to-HBD molar ratio. The two components were thoroughly mixed at a specified temperature using a magnetic stirrer until a clear homogeneous liquid was obtained. The prepared DES was purified by subjecting it to a temperature of 373.15 K in an oven for 8 h to remove traces of impurities and moisture. The obtained solution was stored in an airtight container to prevent exposure to moisture.

Density, viscosity, and refractive index measurements were used to characterize each DES that had been prepared. Measurements of density and refractive index were carried out according to the methods outlined in the literature.[26−28] The refractive index and density were measured using an Atago refractometer (model RX-7000) and an Anton Paar density and sound velocity meter (model DSA 500M), respectively. Prior to DES property measurements, calibration of both pieces of equipment was undertaken by measuring the refractive index and density of ultrapure water at specified temperature.

Measurements of viscosity were carried out according to the method described by Mbatha et al.[29] The viscosity of DES was measured using an Anton Paar AMVn rolling-ball viscometer. Prior to the experimental analysis, ethanol was used to clean the cell, and acetone was used for drying using the automatic Xsample 452 Module. Prior to the viscosity measurements, the water calibration was done at 298.15 K to ensure that the equipment will produce valid results. The uncertainty of ±0.004 was obtained.

Hydrate Liquid−Vapor Equilibrium (HLVE) Data Measurements. *Apparatus.* A schematic diagram of the experimental apparatus which was used in this study is shown in Figure 1. This experimental set up is similar to that which was used by Nkosi et al.[30] The main part of the apparatus is a high-pressure equilibrium cell made of stainless steel (SS 316L) material (supplied by Büchi, Switzerland) with an internal volume of 100 mL. The interior of the cell was hydrophobically coated with an alloy (nickel−chromium−iron−molybdenum) which was capable of withstanding temperatures and pressures up to 473.15 K and 10 MPa, respectively. A four-wire Pt-100 thermocouple (supplied by Grant Instruments, United Kingdom), with an uncertainty of ±0.3 K, was fitted within the cell to monitor the temperature of the system. A pressure transducer (supplied by ESI Technology, United Kingdom) having an uncertainty of ±0.25% of full scale was used to measure the inside pressure of the cell. A magnetic stirrer with a capacity of 1000 rpm was installed to ensure proper mixing of the contents of the cell. A temperature-controlled unit named LTC4 (supplied by Grant Instruments, United Kingdom) consisting of a TX150 Optima circulating bath and an R4 tank/refrigeration unit was used. It allowed to set and control the system temperature, corresponding to the liquid bath temperature. The coolant

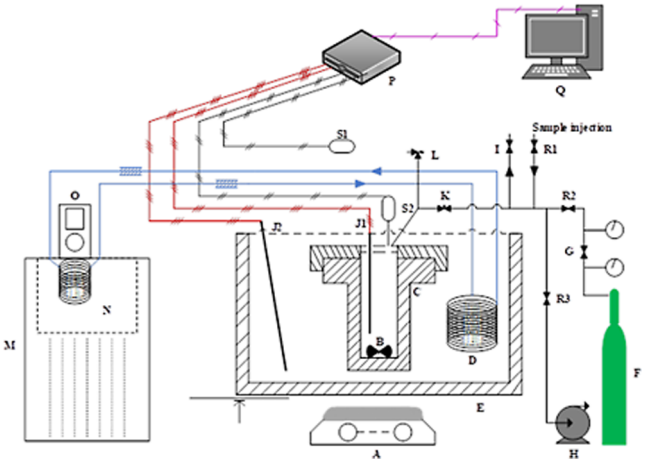

Figure 1. Schematic diagram for the high-pressure equilibrium apparatus: (A) magnetic stirrer; (B) neodymium magnet stir bar; (C) high-pressure equilibrium cell; (D) cooling coil; (E) thermostated bath; (F) gas cylinder; (G) pressure regulator; (H) vacuum pump; (I) vent valve; (J1 and 2) temperature probes (Pt-100); (K) needle valve for loading; (L) relief valve; (M) LTC4 unit; (N) LTC4 unit built-in circulating bath; (O) circulating thermostat; (P) data acquisition system; (Q) computer; (R1−R3) shut-off valve; (S1 and S2) pressure transducers. Reproduced from ref 30. Copyright [2022] American Chemical Society.

was the aqueous solution of glycerol water. Any trapped air inside the cell was removed by a vacuum pump (supplied by Gardner Denver, United States). The apparatus was connected to an SQ2020-1F8 data acquisition unit (supplied by Grant Instruments, United Kingdom) and interfaced with a computer to monitor pressure and temperature data at intervals using SquirrelView software.

Procedure. The dissociation conditions for this study were measured using an isochoric pressure-search method (graphical technique) as described by Sloan and Koh[1] and Tumba et al.[8] The equilibrium cell was evacuated before being fed with the aqueous solution and the gas. After initial evacuation, the appropriate quantity of the aqueous solution (approximately 40 cm^3 with an uncertainty level of ±0.5 cm^3) was injected into the equilibrium cell which was then immersed into the temperature-controlled bath. The gas was then supplied into the cell from a gas cylinder through a pressure regulation valve for gas hydrate formation. After obtaining the stability of temperature and pressure, the valve for the gas line was closed. The system temperature was slowly reduced from the vapor−liquid region which resulted in a slight decrease in pressure. A certain temperature was reached in which the hydrate was formed, and this was detected by a remarkable drop in pressure. After the formation of the hydrate, the temperature was slowly increased in steps of 0.1 K to initiate the dissociation process, and this resulted in a quick rise in pressure. At every temperature step, the temperature was kept constant for a sufficient time to achieve the state of equilibrium within the cell. For each experimental run, a pressure versus temperature diagram was drawn, from which the hydrate dissociation point was obtained. The hydrate dissociation point was the point where the hydrate dissociation trace intersected with the initial cooling trace as shown in Figure 2.

Average Suppression Temperature Calculation. The average suppression temperatures (ΔT_{ave}) of the DESs were calculated to determine the thermodynamic inhibition effects

https://doi.org/10.1021/acs.jced.4c00744
J. Chem. Eng. Data 2025, 70, 3665−3674

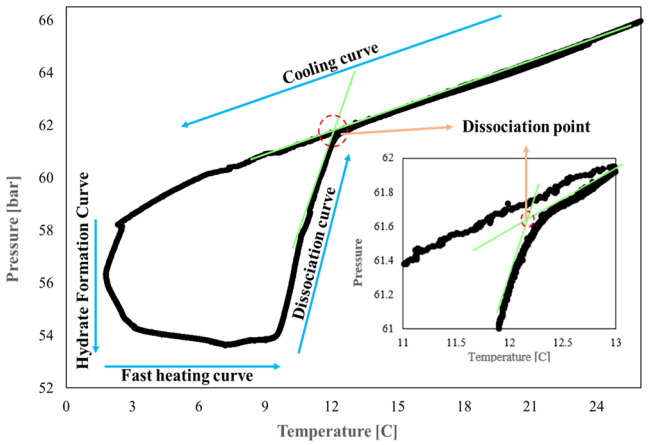

Figure 2. Pressure versus temperature trace for formation and dissociation of the gas hydrate.

of the studied deep eutectic solvents. The inhibition effect is shown in the following equation:[31]

$$\Delta T_{ave} = \frac{\sum \Delta T}{n} = \frac{\sum_{i=0}^{n} (T_0 - T)}{n} \quad (1)$$

where ΔT is defined as the difference between the hydrate dissociation temperature in the absence (T_0) and presence (T) of DESs. The n denotes the number of hydrate dissociation points considered. The values of both dissociation temperatures were obtained from the same dissociation pressure.

Gas Hydrate Dissociation Enthalpy Calculation. The hydrate dissociation enthalpy (ΔH_{diss}) represents the interaction between the host and the guest molecules. A significant change in its magnitude generally indicates a substantial alteration in the hydrate crystalline structure. The hydrate liquid vapor equilibrium data obtained in this worked was used to calculate the gas hydrate dissociation enthalpies according to the Clausius−Clapeyron equation:[1]

$$\frac{d(\ln P)}{d\left(\frac{1}{T}\right)} = -\frac{\Delta H_{diss}}{zR} \quad (2)$$

The left-hand side represents the slope obtained by plotting $\ln(P)$ versus $(1/T)$ values, where P, T, ΔH_{diss}, z, and R are the pressure (MPa), temperature (K), dissociation enthalpy (kJ/mol), compressibility factor, and universal gas constant (J/mol K), respectively.

The compressibility factor (z) was calculated using Pitzer's method:[32]

$$z = z^0 + \omega z^1 \quad (3)$$

where z^0 and z^1 are functions of both the reduced temperature (T_r) and the reduced pressure (P_r) and ω is the acentric factor of the gas. The values of z^0 and z^1 were obtained from the Lee−Kesler generalized correlation.[33] For carbon dioxide and methane, the values of 0.239 and 0.011 for ω were used, respectively.[34]

RESULTS AND DISCUSSION

Characterization of DESs. The characterization of studied DESs was done by measuring their density, viscosity, and refractive index as a function of temperature. The regressions of these properties were performed to explore the effect of temperature on the synthesized DESs. Density is an important property for determining diffusion and miscibility of a solvent with other liquids. The densities of all synthesized DESs were measured at different temperatures that range from 293.15 to 323.15 K and are depicted in Table 4 and Figure 3a. The density of the DES decreased, as the temperature increased for all the DESs. The decrease of the density of the DES as the temperature increased is explained by the increase in the mobility of the DES molecules and the thermal expansion of the DES volume because of the temperature increase. As shown in Table 5, the relationship between the density and temperature is linear with an R^2 value of more than 0.994 for all the DESs. This behavior of density with temperature was also reported for other DES systems in the literature.[35]

Table 4. Density (ρ), Viscosity (μ), and Refractive Index of Tested DESs at a Mole Ratio of 1:3 at T = (293.15−323.15 K) at Atmospheric Pressure[a]

	DES 1			DES 2		
T/K	ρ/g cm^{-3}	μ/mPa s	RI	ρ/g cm^{-3}	μ/mPa s	RI
293.15	1.2094	910.18	1.48861	1.1393	88.31	1.47669
298.15	1.2064	712.05	1.48765	1.1366	73.08	1.47556
303.15	1.2034	544.47	1.48658	1.1335	59.75	1.47435
308.15	1.2003	407.43	1.48542	1.1302	48.33	1.47304
313.15	1.1973	300.94	1.48417	1.1266	38.83	1.47165
318.15	1.1943	225.00	1.48281	1.1227	31.23	1.47017
323.15	1.1913	179.60	1.48136	1.1185	25.54	1.46860
	DES 3			DES 4		
T/K	ρ/g cm^{-3}	μ/mPa s	RI	ρ/g cm^{-3}	μ/mPa s	RI
293.15	1.1692	535.97	1.46690	1.0621	37.39	1.45451
298.15	1.1661	374.94	1.46594	1.0596	30.56	1.45357
303.15	1.1631	268.77	1.46489	1.0571	24.50	1.45253
308.15	1.1594	196.94	1.46375	1.0546	19.21	1.45139
313.15	1.1563	146.83	1.46251	1.0522	14.71	1.45017
318.15	1.1524	112.35	1.46118	1.0498	10.97	1.44884
323.15	1.1497	88.81	1.45975	1.0475	8.01	1.44743

[a]Standard uncertainties are u(T) = 0.05 K, u(P) = 0.1 kPa, u(ρ) = 2 × 10^{-3} g cm^{-3}, and $u(RI)$ = 1.2 × 10^{-3}.

https://doi.org/10.1021/acs.jced.4c00744
J. Chem. Eng. Data 2025, 70, 3665−3674

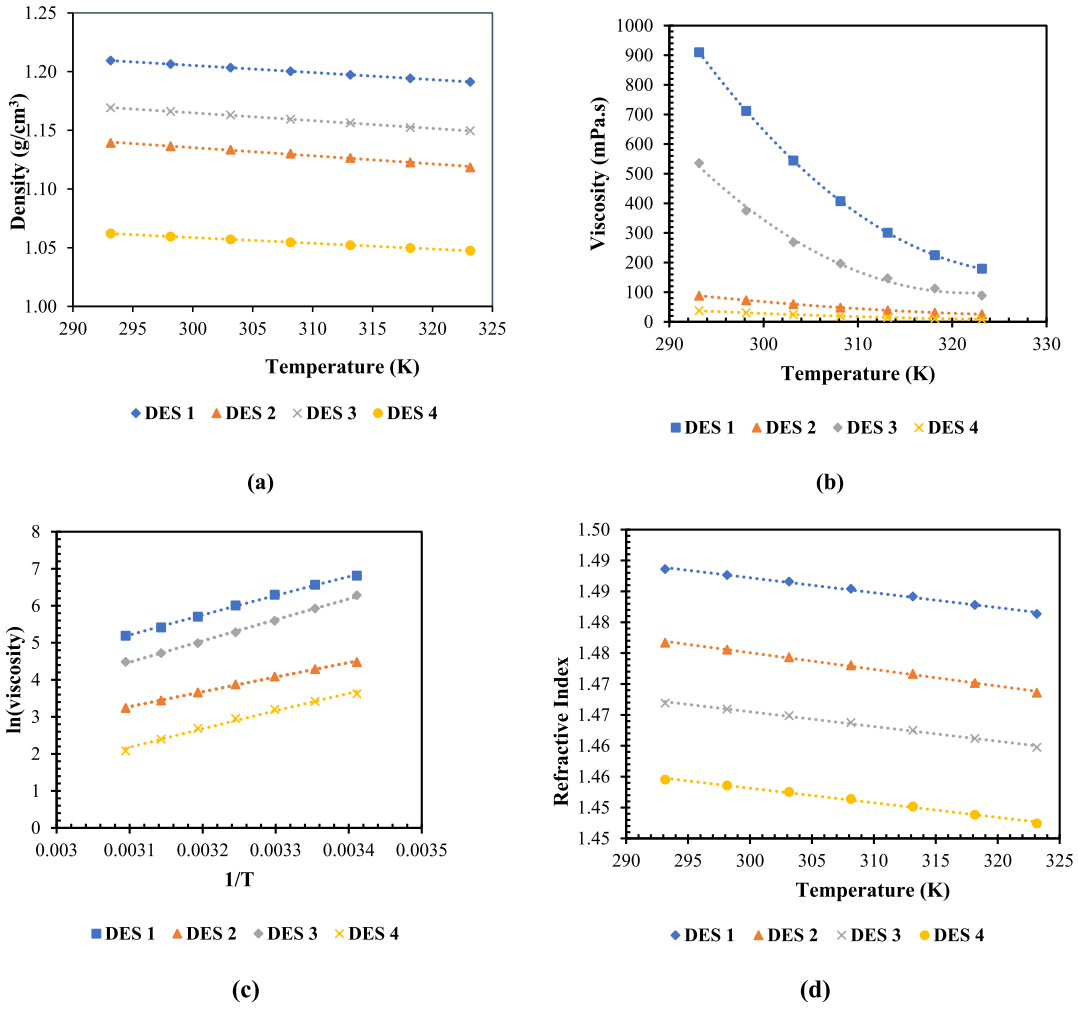

Figure 3. Thermophysical properties of DESs against the temperature range (293.15−323.15) K. (a) Density, (b) viscosity, (c) plot of ln (viscosity) vs $1/T$, and (d) refractive index hydrate liquid−vapor equilibrium (HLVE) data.

Table 5. Regression Analysis of Density (ρ), Viscosity (μ), and Refractive Index versus Temperature Data for Tested DESs over the Temperature Range (293.15−323.15 K)

	R^2		
DES	density	viscosity	refractive index
DES 1	1.0000	0.9984	0.9952
DES 2	0.9948	0.9989	0.9968
DES 3	0.9987	0.9972	0.9953
DES 4	0.9998	0.9915	0.9952

Similarly, the viscosity is also strongly affected by changes in temperature. The viscosities of DESs were also measured as a function of temperature and are shown in Table 4 and Figure 3b. It is observed that the viscosity values decrease as the temperature increases from 293.15 to 323.15 K. This is due to the mobility of ions as a result of increased temperature which weakens the intermolecular interaction between the molecules and ions within the fluid.[36] The regression analysis for viscosity as a function of temperature was based on graph plotting of ln (viscosity) versus $1/T$, as shown in Figure 3c. There is a strong relation (R^2 >0.991) between the viscosity and temperature for all DES samples, as shown in Table 5. This behavior of viscosity with temperature was also reported for other DES systems in the literature.[37]

Refractive index (RI) is a physical property that is used to characterize a new solvent due to its association with the electrical permittivity and magnetic permeability of the materials. It is a critical property that reflects the purity of a solvent or concentration of components. For pure DESs, RI is found to decrease linearly with temperature.[37] The RIs of all the studied DESs were measured as a function of temperature and are presented in Table 4 and Figure 3d. Like the observation in the case of density and viscosity, the RIs for all the DES decreased with an increase in temperature. This is because the density decreases with an increase in temperature, thus allowing more freedom of the movement of light that reduces the refractive index. A strong linear relationship (R^2 >0.995) between RI and temperature was exhibited by all DES samples, as shown in Table 5. This behavior of RI with temperature was also observed for other DES systems in the literature.[38]

Hydrate Liquid-Vapor Equilibrium (HLVE) Data. All the measured hydrate liquid−vapor equilibrium data are reported in Table 6 and plotted in Figures 4 and 5. Some selected experimental data from the literature on the dissociation conditions of carbon dioxide and methane clathrate hydrates in the presence of pure water are also presented.[30,39] The reliability of the experimental procedure used was examined before producing the hydrate phase

https://doi.org/10.1021/acs.jced.4c00744
J. Chem. Eng. Data 2025, 70, 3665−3674

Table 6. Phase Equilibrium Data of CO_2 and CH_4 in Water with and without 2 wt % and 4 wt % Aqueous DES Solutions[a]

water		DES 1		DES 2		DES 3		DES 4	
T (K)	P (MPa)	T (K)	P (MPa)	T (K)	P (MPa)	T (K)	P (MPa)	T (K)	P (MPa)
				CO_2 + 2 wt % DES + water					
277.85	2.03	277.98	2.22	278.29	2.27	277.90	2.41	278.00	2.32
279.19	2.42	279.40	2.81	279.59	2.80	279.16	2.91	279.42	2.92
280.69	3.14	280.83	3.45	280.64	3.28	280.17	3.36	280.40	3.35
281.76	3.67	281.84	3.94	282.20	4.02	281.55	4.09	281.94	4.18
282.77	4.20	282.85	4.49	282.89	4.35	282.97	4.91	282.88	4.71
				CO_2 + 4 wt % DES + water					
277.85	2.03	278.13	2.57	277.96	2.40	277.90	2.35	278.05	2.64
279.19	2.42	278.80	2.86	279.29	2.93	279.66	3.51	278.93	3.00
280.69	3.14	279.78	3.31	280.25	3.37	280.64	4.01	280.59	3.79
281.76	3.67	280.89	3.85	281.09	3.80	281.73	4.64	281.47	4.29
282.77	4.20	282.66	4.81	282.75	4.75	282.80	5.28	282.75	5.02
				CH_4 + 2 wt % DES + water					
276.92	3.81	277.04	4.08	276.89	3.81	276.54	4.03	276.70	3.94
279.22	4.77	278.68	5.03	278.45	4.66	279.16	5.62	279.38	5.57
281.42	6.06	280.45	6.11	280.72	6.03	281.35	7.08	281.94	7.26
282.52	6.77	282.55	7.49	282.37	7.10	282.23	7.70	282.84	7.88
284.21	8.12	283.50	8.16	283.45	7.83	283.14	8.36	283.78	8.56
285.15	8.90	284.85	9.05	284.80	8.75	284.98	9.76	285.00	9.44
				CH_4 + 4 wt % DES + water					
276.92	3.81	276.25	3.92	276.18	3.71	276.03	4.06	276.53	4.22
279.22	4.77	277.92	4.94	278.73	5.25	278.33	5.58	278.21	5.32
281.42	6.06	279.64	6.02	280.48	6.34	280.89	7.38	279.93	6.48
282.52	6.77	281.58	7.25	281.50	6.99	282.37	8.48	281.87	7.81
284.21	8.12	283.19	8.40	283.50	8.36	283.88	9.64	283.48	9.05
285.15	8.90	284.78	9.53	284.70	9.22	284.85	10.39	284.80	10.06

[a]Standard uncertainty: $u(T)$ (0.95 level of confidence) = ±0.08 K, $u(P)$ (0.95 level of confidence) = ±0.0234 MPa K, and u (DES molar ratio) = 0.005.

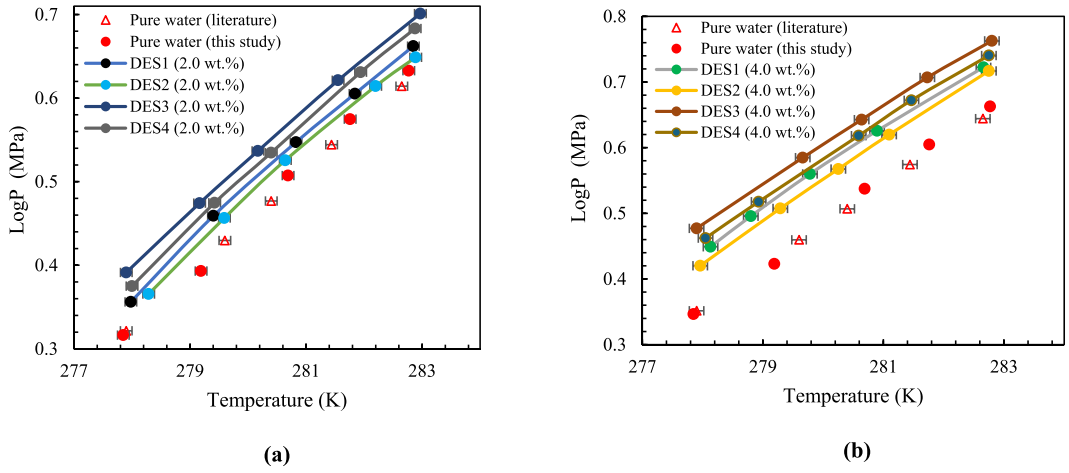

Figure 4. Thermodynamic stability condition curves for the CO_2 + H_2O system in the presence and absence of DESs: (a) 2 wt % DES and (b) 4 wt % DES. The pure water data was taken from the literature.[30]

equilibrium data reported in this study and it is demonstrated by the reasonable agreement between the experimental data from this study and those reported in the literature as shown in Figures 5 and 6. The HLVE data were measured at 2 and 4 wt % concentrations of DES in an aqueous solution. The inhibition effect of a thermodynamic hydrate inhibitor is evident through the shifting of hydrate dissociation conditions to higher pressure and lower temperature regions.[5,8] It is observed from Figures 5 and 6 that all four studied DESs have thermodynamic inhibition effects on clathrate hydrates of carbon dioxide and methane by moving HLVE to higher pressure and lower temperature regions in comparison to that of a pure water HLVE curve. This thermodynamic inhibition effect on carbon dioxide and methane hydrates is dependent on the concentration of DES in the aqueous solution and is independent of the type of clathrate hydrate former. The activity of DES in the aqueous phase is increased due to the increase in concentration of the solution. Higher inhibition ability is observed at 4 wt % concentration in comparison to that of 2 wt % because of the increased activity of DES. From

https://doi.org/10.1021/acs.jced.4c00744
J. Chem. Eng. Data 2025, 70, 3665−3674

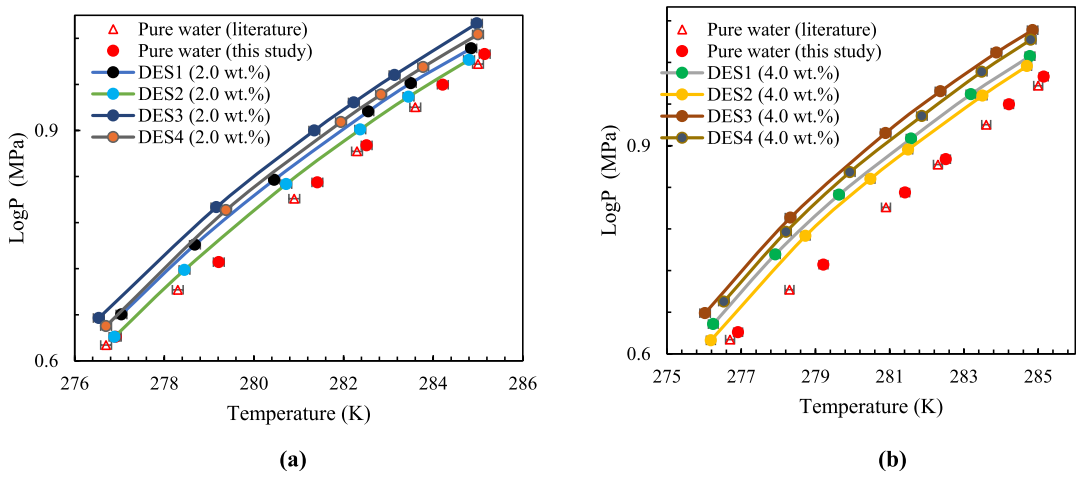

Figure 5. Thermodynamic stability condition curves for the CH_4 + H_2O system with and without DES inclusion: (a) 2 wt % DES and (b) 4 wt % DES. The pure water data was taken from the literature.[39]

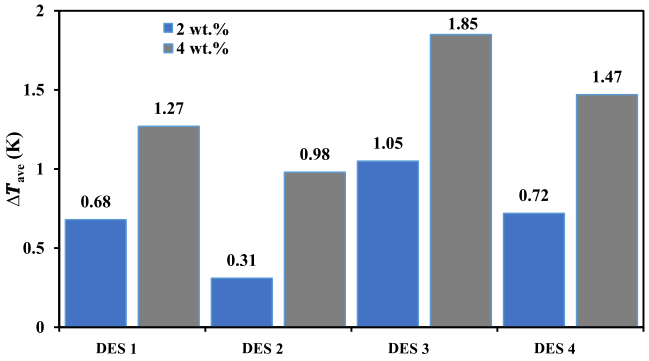

Figure 6. Average temperatures of the studied DESs for the CO_2 gas system.

all four DESs, DES 3 showed the maximum shift of the equilibrium boundary of water with DES 2 displaying the minimum shift. The gas hydrate inhibition ability arranged from the highest to the lowest is TMAC/glycerol (DES 3) > TMAC/EG (DES 4) > TPAB/glycerol (DES 1) > TPAB/EG (DES 2). The superiority of DES 3 over the rest of the DESs could be due to the nature of its pure components. From the pattern observed, it is evident that for HBAs, TMAC is superior to TPAB, while glycerol is superior to ethylene glycol for HBDs. A fundamental requirement for a substance to be an effective thermodynamic hydrate inhibitor is its potential to form hydrogen bonds with water molecules.[10] These DESs have great potential to be effective thermodynamic hydrate inhibitors because they have tunable properties which can be designed to form hydrogen bonding with water.

Average Suppression Temperatures (ΔT_{ave}). To compare the impact of studied DESs on thermodynamic hydrate inhibition performance on carbon dioxide and methane gas hydrates, the average suppression temperatures (ΔT_{ave}) were also calculated for 2 and 4 wt % DES solutions. The results are tabulated in Tables 7 and 8 and graphically presented in Figures 6 and 7.

The thermodynamic hydrate inhibition impact is found to be in the order of: TMAC/glycerol (DES 3) > TMAC/EG (DES 4) > TPAB/glycerol (DES 1) > TPAB/EG (DES 2). From this pattern, it is also evident for HBAs that TMAC performs better than TPAB, while for HBDs, glycerol is better than ethylene glycol. For the carbon dioxide system, the degree of suppression achieved by the combination of TMAC and glycerol (DES 3) is 1.05 K at 2 wt % and 1.85 K at 4 wt %, whereas for the CH_4 system, it is 1.43 K at 2 wt % and 2.18 K at 4 wt %. The best performance of TMAC can be attributed to its shorter alkyl chain as compared to TPAB. The results are in line with the previously reported data for quaternary ammonium salts and ionic liquids, alkyl chain lengths of these substances affect the phase stability of hydrate formation.[40,41] The main reason for this is that the longer alkyl chain length leads to hydrophobicity and it does not allow the cationic part of ionic liquid to bond with the hydroxyl ion.[4] The superiority of glycerol over ethylene glycol is based on the presence of three hydroxyl (OH) groups in glycerol as compared to two in ethylene glycol. Increasing the number of

Table 7. Average Suppression Temperature Data at Different Pressure Conditions for the CO_2 Gas System

	DES 1		DES 2		DES 3		DES 4	
P (MPa)	ΔT (K)		ΔT (K)		ΔT (K)		ΔT (K)	
	2 wt %	4 wt %	2 wt %	4 wt %	2 wt %	4 wt %	2 wt %	4 wt %
2.0	0.55	1.21	0.14	0.78	0.88	1.73	0.52	1.30
2.5	0.91	1.42	0.51	1.17	1.24	2.04	0.66	1.67
3.0	0.72	1.29	0.37	0.96	1.04	1.90	0.79	1.48
3.5	0.65	1.31	0.36	0.97	1.05	1.83	0.78	1.48
4.0	0.69	1.27	0.32	1.02	1.06	1.82	0.82	1.48
4.5	0.58	1.10	0.16	0.99	1.01	1.79	0.76	1.42
ΔT_{ave} (K)	**0.68**	**1.27**	**0.31**	**0.98**	**1.05**	**1.85**	**0.72**	**1.47**

https://doi.org/10.1021/acs.jced.4c00744
J. Chem. Eng. Data 2025, 70, 3665−3674

Table 8. Average Suppression Temperature Data for the CH_4 Gas System

P (MPa)	DES 1		DES 2		DES 3		DES 4	
	ΔT (K)		ΔT (K)		ΔT (K)		ΔT (K)	
	2 wt %	4 wt %	2 wt %	4 wt %	2 wt %	4 wt %	2 wt %	4 wt %
4.00	0.46	0.98	0.13	0.70	0.89	1.43	0.57	1.18
4.75	0.97	1.55	0.57	1.25	1.45	2.09	1.14	1.83
5.50	1.07	1.67	0.68	1.39	1.57	2.32	1.27	2.04
6.25	1.05	1.71	0.65	1.38	1.62	2.42	1.29	2.11
7.00	0.94	1.62	0.59	1.29	1.58	2.46	1.26	2.12
7.75	0.83	1.47	0.42	1.10	1.45	2.36	1.10	1.97
ΔT_{ave} (K)	**0.89**	**1.50**	**0.51**	**1.19**	**1.43**	**2.18**	**1.11**	**1.88**

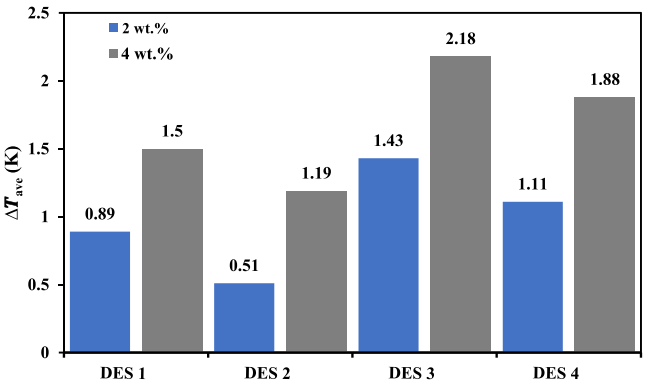

Figure 7. Average temperatures of the studied DESs for the CH_4 gas system.

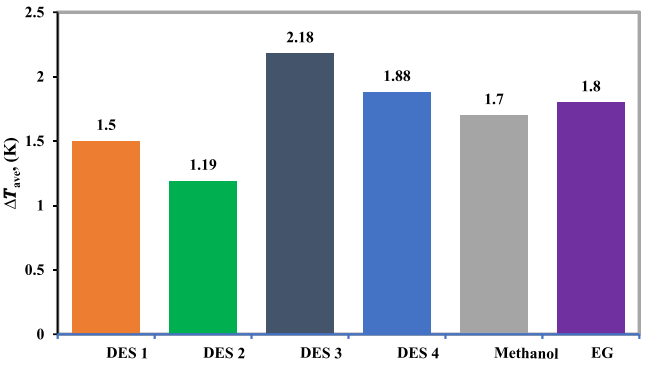

Figure 8. Comparison of the inhibition effects of the studied DESs on CH_4 hydrates with commercial THIs, methanol, and ethylene glycol (obtained from the literature[42]). The mass and molar concentrations of inhibitors are DES 1—4 wt % (0.68 mol %), DES 2—4 wt % (0.97 mol %), DES 3—4 wt % (0.78 mol %), DES 4—4 wt % (1.07 mol %), methanol—4.2 wt % (2.40 mol %), and ethylene glycol—6.9 wt % (2.10 mol %).

hydroxyl groups on a molecule generally enhances its ability to inhibit gas hydrate formation. This is because hydroxyl groups can form hydrogen bonds with water molecules in the hydrate structure, disrupting the lattice, thereby hindering hydrate formation.

Table 9 shows the average suppression temperatures of commercial thermodynamic inhibitors (methanol and ethylene glycol) calculated from the phase equilibrium data that was obtained from the literature.[42] For comparative analysis, Figure 8 represents the average suppression temperatures at 4 wt % of the studied systems with the commercial thermodynamic inhibitors. The inhibition performance of DES 3 and DES 4 seems to be superior to the commercial THIs; however, various combinations of DESs in future studies would give comparable results in the light of relevant concentration levels. A better performance of these DESs may be attributed to the synergistic effect which arises due to the combination of two inhibitors which produces an inhibition effect that is greater than the sum of their individual behavior.

Table 9. Average Suppression Temperature Data of Commercial Thermodynamic Inhibitors (Methanol and Ethylene Glycol) for the CH_4 Gas System

	methanol	ethylene glycol
	4.2 wt % (2.40 mol %)	6.9 wt % (2.10 mol %)
P (MPa)	ΔT (K)	ΔT (K)
4.00	1.74	1.95
4.75	1.77	1.96
5.50	1.63	1.82
6.25	1.71	1.72
7.00	1.69	1.73
7.75	1.66	1.60
ΔT_{ave} (K)	**1.70**	**1.80**

Gas Hydrate Dissociation Enthalpies (ΔH_{diss}). To evaluate the participation of DESs in the hydrate crystalline structure, the gas hydrate dissociation enthalpies (ΔH_{diss}) of all studies systems were calculated via the Clausius−Clapeyron equation. The ΔH_{diss} data of carbon dioxide and methane systems are presented in Tables 10 and 11, respectively.

It is well known that carbon dioxide and methane form structure I gas hydrates.[43,44] The dissociation enthalpy of hydrates is mainly altered by the hydrogen bonding of the clathrate structure and cage occupancy of the guest molecule.[45] As displayed in Tables 10 and 11, it is evident from the results obtained that DES molecules did not contribute to the hydrate crystallization process as the dissociation enthalpy values did not significantly change in their presence as compared to pure water. Thus, it can be inferred that the thermodynamic hydrate inhibition behavior shown by the studied DESs is primarily due to their hydrogen-bonding ability.

CONCLUSIONS

In this work, the thermodynamic inhibition behavior of four DESs has been investigated for carbon dioxide and methane gas hydrates. The DESs were made at a 1:3 molar ratio for the combinations of TPAB/Glycerol, TPAB/EG, TMAC/Glycerol, and TMAC/EG. It was shown that all four studied DESs have inhibition effects on the clathrate hydrates of carbon dioxide and methane in the concentration ranges investigated in this work. This inhibition effect was dependent on the

https://doi.org/10.1021/acs.jced.4c00744
J. Chem. Eng. Data 2025, 70, 3665−3674

Table 10. Dissociation Enthalpies (ΔH_{diss}) of DESs in the CO_2 Gas System

		DES 1		DES 2		DES 3		DES 4	
P (MPa)	pure H_2O	2 wt %	4 wt %	2 wt %	4 wt %	2 wt %	4 wt %	2 wt %	4 wt %
2.0	84.81	83.33	82.05	83.87	85.72	84.59	82.76	88.36	84.09
2.5	81.99	80.47	79.24	81.02	82.77	81.68	79.89	85.38	81.18
3.0	79.17	77.70	76.48	78.23	79.92	78.86	77.09	82.38	78.35
3.5	76.42	75.00	73.78	75.51	77.11	76.09	74.36	79.50	75.58
4.0	73.72	72.31	71.13	72.84	74.33	73.35	71.66	76.64	72.85
4.5	71.04	69.69	68.54	70.23	71.59	70.65	68.99	73.84	70.15
$\Delta H_{dissave}$ (kJ/mol)	77.86	76.42	75.20	76.95	78.57	77.54	75.79	81.02	77.05

Table 11. Dissociation Enthalpies (ΔH_{diss}) of DESs in the CH_4 Gas System

		DES 1		DES 2		DES 3		DES 4	
P (MPa)	pure H_2O	2 wt %	4 wt %	2 wt %	4 wt %	2 wt %	4 wt %	2 wt %	4 wt %
4.00	62.21	64.73	65.89	64.54	65.13	66.82	70.96	66.65	69.36
4.75	61.24	63.67	64.80	63.50	64.05	65.72	69.77	65.55	68.20
5.50	60.28	62.64	63.74	62.48	63.01	64.65	68.61	64.49	67.08
6.25	59.33	61.65	62.71	61.49	62.00	63.60	67.49	63.46	65.98
7.00	58.40	60.68	61.72	60.53	61.03	62.59	66.39	62.45	64.91
7.75	57.48	59.72	60.74	59.58	60.07	61.60	65.31	61.47	63.88
$\Delta H_{dissave}$ (kJ/mol)	59.82	62.18	63.27	62.02	62.55	64.16	68.09	64.01	66.57

concentration of DES in the aqueous solution but independent of the type of clathrate hydrate former. The gas hydrate inhibition ability ranked from the highest to the lowest was found to be in the order of: TMAC/glycerol (DES 3) > TMAC/EG (DES 4) > TPAB/glycerol (DES 1) > TPAB/EG (DES 2). The superiority of DES 3 over the rest of the DESs could mainly be due to the nature of its pure components. From the pattern observed, it is evident that for HBA components, TMAC was superior to TPAB, whereas for HBD components, glycerol was superior to ethylene glycol. The best performance of TMAC as HBA compared to its counterpart TPAB can be attributed to its shorter alkyl chain. The average suppression temperatures ranged between 0.31 and 2.18 K. This study demonstrated the potential of DESs to be an ultimate alternative to the currently available conventional THIs. Therefore, further studies are needed for enhanced tuning of DESs as thermodynamic hydrate inhibitors.

AUTHOR INFORMATION

Corresponding Author

Njabulo Mziwandile Zulu − *School of Chemical and Metallurgical Engineering, Oil and Gas Production and Processing Research Unit, University of the Witwatersrand, Johannesburg 2001, South Africa; Department of Chemical Engineering, Thermodynamics, Materials and Separations Research Group (TMSRG), Mangosuthu University of Technology, Durban 4001, South Africa;* orcid.org/0009-0005-5538-697X; Email: zulunm@mut.ac.za

Authors

Hamed Hashemi − *School of Chemical and Metallurgical Engineering, Oil and Gas Production and Processing Research Unit, University of the Witwatersrand, Johannesburg 2001, South Africa*

Kaniki Tumba − *Department of Chemical and Mineral Engineering, Faculty of Engineering, North-West University, Potchefstroom 2531, South Africa;* orcid.org/0000-0003-2685-3741

Complete contact information is available at: https://pubs.acs.org/10.1021/acs.jced.4c00744

Author Contributions

The manuscript was written through contributions of all authors. Njabulo Mziwandile Zulu: Conceptualization, methodology, investigation, writing—original draft, review, and editing. Hamed Hashemi: Supervision and contribution to the review and editing of the original draft. Kaniki Tumba: Supervision, project administration, funding acquisition, and review and editing of the original draft.

Notes

The authors declare no competing financial interest.

ACKNOWLEDGMENTS

This study has been supported by the Mangosuthu University of Technology (MUT) and Witwatersrand University. The Mangosuthu University of Technology is appreciated for the financial support while undertaking this research project. The authors would like to, respectively, appreciate S.S. Dladla and Dr N. Nkosi for their assistance with experimental data acquisition and graphical presentation.

REFERENCES

(1) Sloan, E. D.; Koh, C. A. *Clathrate Hydrates of Natural Gases*, 3rd ed.; CRC Press, Taylor & Francis Group: Boca Raton, FL, 2008.

(2) Hammerschmidt, E. G. Formation of Gas Hydrates in Natural Gas Transmission Lines. *Ind. Eng. Chem.* **1934**, *26* (8), 851−855.

(3) Tariq, M.; Rooney, D.; Othman, E.; Aparicio, S.; Atilhan, M.; Khraisheh, M. Gas Hydrate Inhibition: A Review of the Role of Ionic Liquids. *Ind. Eng. Chem. Res.* **2014**, *53* (46), 17855−17868.

(4) Qasim, A.; Khan, M. S.; Lal, B.; Shariff, A. M. Phase Equilibrium Measurement and Modeling Approach to Quaternary Ammonium Salts with and without Monoethylene Glycol for Carbon Dioxide Hydrates. *J. Mol. Liq.* **2019**, *282*, 106−114.

(5) Patel, Z. D.; Russum, J. Flow Assurance: Chemical Inhibition of Gas Hydrates in Deepwater Production Systems. *Offshore* **2010**, *70* (6), 70−73.

(6) Cha, M.; Shin, K.; Kim, J.; Chang, D.; Seo, Y.; Lee, H.; Kang, S. P. Thermodynamic and Kinetic Hydrate Inhibition Performance of

Aqueous Ethylene Glycol Solutions for Natural Gas. *Chem. Eng. Sci.* **2013**, *99*, 184−190.
(7) Kanda, H.; Uchida, K.; Nakamura, K.; Suzuki, T. Economics and Energy Requirements on Natural Gas Ocean Transportation in Form of Natural Gas Hydrate (NGH) Pellets. In *Proceedings of Fifth International Conference on Gas Hydrate*, 2005, pp 1275−1282.
(8) Tumba, K.; Reddy, P.; Naidoo, P.; Ramjugernath, D.; Eslamimanesh, A.; Mohammadi, A. H.; Richon, D. Phase Equilibria of Methane and Carbon Dioxide Clathrate Hydrates in the Presence of Aqueous Solutions of Tributylmethylphosphonium Methylsulfate Ionic Liquid. *J. Chem. Eng. Data* **2011**, *56* (9), 3620−3629.
(9) Brustad, S.; Løken, K.-P.; Waalmann, J. G. Hydrate Prevention Using MEG Instead of MeOH: Impact of Experience from Major Norwegian Developments on Technology Selection for Injection and Recovery of MEG. In *Offshore Technology Conference; Offshore Technology Conference*, 2005..
(10) Xiao, C.; Adidharma, H. Dual Function Inhibitors for Methane Hydrate. *Chem. Eng. Sci.* **2009**, *64* (7), 1522−1527.
(11) Chen, L.; Sharifzadeh, M.; Mac Dowell, N.; Welton, T.; Shah, N.; Hallett, J. P. Inexpensive Ionic Liquids: [HSO_4]—Based Solvent Production at Bulk Scale. *Green Chem.* **2014**, *16* (6), 3098−3106.
(12) Thuy Pham, T. P.; Cho, C.-W.; Yun, Y.-S. Environmental Fate and Toxicity of Ionic Liquids: A Review. *Water Res.* **2010**, *44* (2), 352−372.
(13) Smiglak, M.; Reichert, W. M.; Holbrey, J. D.; Wilkes, J. S.; Sun, L.; Thrasher, J. S.; Kirichenko, K.; Singh, S.; Katritzky, A. R.; Rogers, R. D. Combustible Ionic Liquids by Design: Is Laboratory Safety Another Ionic Liquid Myth? *Chem. Commun.* **2006**, *24*, 2554.
(14) Biczak, R.; Pawłowska, B.; Bałczewski, P.; Rychter, P. The Role of the Anion in the Toxicity of Imidazolium Ionic Liquids. *J. Hazard. Mater.* **2014**, *274*, 181−190.
(15) Paduszyński, K.; Domańska, U. Viscosity of Ionic Liquids: An Extensive Database and a New Group Contribution Model Based on a Feed-Forward Artificial Neural Network. *J. Chem. Inf. Model.* **2014**, *54* (5), 1311−1324.
(16) Kudłak, B.; Owczarek, K.; Namieśnik, J. Selected Issues Related to the Toxicity of Ionic Liquids and Deep Eutectic Solvents—a Review. *Environ. Sci. Pollut. Res.* **2015**, *22* (16), 11975−11992.
(17) Zhang, Q.; De Oliveira Vigier, K.; Royer, S.; Jérôme, F. Deep Eutectic Solvents: Syntheses, Properties and Applications. *Chem. Soc. Rev.* **2012**, *41* (21), 7108.
(18) Sivabalan, V.; Sahith, J. K.; Lal, B. Deep Eutectic Solvents as the New Norm for Oil and Gas Industry: A Mini Review. In *Proceedings of the Third International Conference on Separation Technology 2020 (ICoST 2020)*; Atlantis Press: Paris, France, 2020..
(19) Lee, D.; Go, W.; Oh, J.; Lee, J.; Jo, I.; Kim, K.-S.; Seo, Y. Thermodynamic Inhibition Effects of an Ionic Liquid (Choline Chloride), a Naturally Derived Substance (Urea), and Their Mixture (Deep Eutectic Solvent) on CH4 Hydrates. *Chem. Eng. J.* **2020**, *399*, 125830.
(20) Sivabalan, V.; Hasnor, N.; Lal, B.; Kassim, Z.; Shah Maulud, A. Tetraethylammonium Acetate and Tetraethylammonium Bromide-Based Deep Eutectic Solvents as Thermodynamic CO2 Gas Hydrate Inhibitors. *Appl. Sci.* **2020**, *10* (19), 6794.
(21) Khoo, Y. Z.; Ho, Y.-H.; Chang, K.-Y.; Chen, Y.-P.; Chen, L.-J. Dual Inhibition Effect of Reline Deep Eutectic Solvent on Methane Hydrate Nucleation and Formation. *Fuel* **2022**, *328*, 125376.
(22) Rasool, M. H.; Zamir, A.; Elraies, K. A.; Ahmad, M.; Ayoub, M.; Abbas, M. A. A Deep Eutectic Solvent Based Novel Drilling Mud with Modified Rheology for Hydrates Inhibition in Deep Water Drilling. *J. Pet. Sci. Eng.* **2022**, *211*, 110151.
(23) Abbott, A. P.; Capper, G.; Davies, D. L.; Rasheed, R. K.; Tambyrajah, V. Novel Solvent Properties of Choline Chloride/Urea Mixtures. *Chem. Commun.* **2003**, No. 1, 70−71.
(24) Smith, E. L.; Abbott, A. P.; Ryder, K. S. Deep Eutectic Solvents (DESs) and Their Applications. *Chem. Rev.* **2014**, *114* (21), 11060−11082.
(25) Verevkin, S. P.; Sazonova, A. Y.; Frolkova, A. K.; Zaitsau, D. H.; Prikhodko, I. V.; Held, C. Separation Performance of BioRenewable Deep Eutectic Solvents. *Ind. Eng. Chem. Res.* **2015**, *54* (13), 3498−3504.
(26) Nkosi, N.; Tumba, K.; Ramsuroop, S. Measurements of Activity Coefficient at Infinite Dilution for Organic Solutes in Tetramethylammonium Chloride + Ethylene Glycol Deep Eutectic Solvent Using Gas-Liquid Chromatography. *Fluid Phase Equilib.* **2018**, *462*, 31−37.
(27) Nkosi, N.; Tumba, K.; Ramsuroop, S. Tetramethylammonium Chloride + Glycerol Deep Eutectic Solvent as Separation Agent for Organic Liquid Mixtures: Assessment from Experimental Limiting Activity Coefficients. *Fluid Phase Equilib.* **2018**, *473*, 98−105.
(28) Nkosi, N.; Tumba, K.; Ramsuroop, S. Activity Coefficients at Infinite Dilution of Various Organic Solutes in the Deep Eutectic Solvent (Tetramethylammonium Chloride + 1,6 Hexanediol in the 1:1 Molar Ratio). *South African J. Chem. Eng.* **2019**, *27*, 7−15.
(29) Mbatha, B. P.; Ngema, P. T.; Nkosi, N.; Ramsuroop, S. Infinite Dilution Activity Coefficient Measurements for 1-Methyl-4-(1-Methylethenyl)-Cyclohexene as a Green Solvent for Separation. *J. Chem. Eng. Data* **2022**, *67* (4), 966−974.
(30) Nkosi, N.; Nkazi, D.; Tumba, K. Experimental Hydrate Phase Equilibrium Data Relevant to Bitter Melon, Pineapple, and Grape Juice Concentration. *ACS Omega* **2022**, *7* (39), 34741−34751.
(31) Xiao, C.; Wibisono, N.; Adidharma, H. Dialkylimidazolium Halide Ionic Liquids as Dual Function Inhibitors for Methane Hydrate. *Chem. Eng. Sci.* **2010**, *65* (10), 3080−3087.
(32) Smith, J. M.; Van Ness, H. C.; Abbott, M. M.; Swihart, M. T. *Introduction to Chemical Engineering Thermodynamics*, 8th ed.; 2018.
(33) Lee, B. I.; Kesler, M. G. A Generalized Thermodynamic Correlation Based on Three-parameter Corresponding States. *AIChE J.* **1975**, *21* (3), 510−527.
(34) Reid, R. C.; Prausnitz, J. M.; Poling, B. E. *The Properties of Gases and Liquids*, 4th ed.; McGraw-Hill: New York, 1987.
(35) Jibril, B.; Mjalli, F.; Naser, J.; Gano, Z. New Tetrapropylammonium Bromide-Based Deep Eutectic Solvents: Synthesis and Characterizations. *J. Mol. Liq.* **2014**, *199*, 462−469.
(36) Ramírez Verduzco, L. F. Density and Viscosity of Biodiesel as a Function of Temperature: Empirical Models. *Renew. Sustain. Energy Rev.* **2013**, *19*, 652−665.
(37) Rosmi, S. N. A. B. *Synthesis and Characterization of Deep Eutectic Solvents (DESs)*; Universiti Teknologi PETRONAS, 2015.
(38) Mjalli, F. S.; Naser, J.; Jibril, B.; Al-Hatmi, S. S.; Gano, Z. S. Ionic Liquids Analogues Based on Potassium Carbonate. *Thermochim. Acta* **2014**, *575*, 135−143.
(39) Adisasmito, S.; Frank, R. J.; Sloan, E. D. Hydrates of Carbon Dioxide and Methane Mixtures. *J. Chem. Eng. Data* **1991**, *36* (1), 68−71.
(40) Gupta, P.; Chandrasekharan Nair, V.; Sangwai, J. S. Phase Equilibrium of Methane Hydrate in the Presence of Aqueous Solutions of Quaternary Ammonium Salts. *J. Chem. Eng. Data* **2018**, *63* (7), 2410−2419.
(41) Khan, M. S.; Lal, B.; Keong, L. K.; Sabil, K. M. Experimental Evaluation and Thermodynamic Modelling of AILs Alkyl Chain Elongation on Methane Riched Gas Hydrate System. *Fluid Phase Equilib.* **2018**, *473*, 300−309.
(42) Mohammadi, A. H.; Richon, D. Phase Equilibria of Methane Hydrates in the Presence of Methanol and/or Ethylene Glycol Aqueous Solutions. *Ind. Eng. Chem. Res.* **2010**, *49* (2), 925−928.
(43) Khan, M. S.; Bavoh, C. B.; Partoon, B.; Nashed, O.; Lal, B.; Mellon, N. B. Impacts of Ammonium Based Ionic Liquids Alkyl Chain on Thermodynamic Hydrate Inhibition for Carbon Dioxide Rich Binary Gas. *J. Mol. Liq.* **2018**, *261*, 283−290.
(44) Qasim, A.; Khan, M. S.; Lal, B.; Ismail, M. C.; Rostani, K. Quaternary Ammonium Salts as Thermodynamic Hydrate Inhibitors in the Presence and Absence of Monoethylene Glycol for Methane Hydrates. *Fuel* **2020**, *259*, 116219.
(45) Sloan, E. D.; Koh, C. A.; Sum, A. K. Gas Hydrate Stability and Sampling: The Future as Related to the Phase Diagram. *Energies* **2010**, *3* (12), 1991−2000.

https://doi.org/10.1021/acs.jced.4c00744
J. Chem. Eng. Data 2025, 70, 3665−3674